Extreme Mechanics Letters 17 (2017) 56–61

Contents lists available at ScienceDirect

Extreme Mechanics Letters

journal homepage: www.elsevier.com/locate/eml

Elastic architected materials with extreme damping capacity

Babak Haghpanah, Ahmad Shirazi, Ladan Salari-Sharif, Anna Guell Izard, Lorenzo Valdevit *

Department of Mechanical and Aerospace Engineering, University of California, Irvine, United States

ARTICLE INFO

Article history:
Received 19 July 2017
Received in revised form 23 September 2017
Accepted 29 September 2017
Available online 9 October 2017

ABSTRACT

We report on a new class of elastic architected materials with hybrid unit cells, consisting of discrete elastic elements with non-convex strain energy and one convex (but possibly nonlinear) elastic element, to obtain a reversible multifunctional material with extreme energy dissipation. The proposed design exploits numerically optimized nonlinearities in the force–displacement response of the sub-unit-cell elements to approach the theoretical limit of specific damping capacity in any material, $\psi^{th} = 8$. Specific damping capacities up to $\psi = 6.02$ were experimentally demonstrated, which are far greater than any experimental value previously reported, including in high damping elastomers ($\psi < 4.5$). Remarkably, this damping performance is achieved even with a single unit cell, thus avoiding the need for thick multi-cell designs. Furthermore, the proposed design offers relatively high stiffness and low transmitted stress upon compression. The proposed concept could enable the design of reversible impact-resistant structures with superior crashworthiness and energy dissipation.

1. Introduction

Architected materials encompassing elements with non-convex strain energy landscapes have recently been touted as promising candidates for the implementation of future reusable energy trapping and impact protection systems [1–3], multi-stable shape shifting materials [4–7], advanced dampers and vibration isolation devices [8–12], and stable transition wave diodes [13,14]. Even though these materials are capable of dissipating strain energy while remaining elastic, which can result in reversible deformations and long life span, their relatively small hysteresis hinders their application for vibration damping and impact absorption [3,8,15]. The magnitude of energy dissipation under cyclic or non-cyclic (e.g., impact) loading can be nonlinearly enhanced by connecting a large number of negative stiffness (NS) elements in series, but this generally results in thick and heavy structures [2]. Recent developments have allowed achievement of high damping in similar architected elastic systems, such as hollow metallic micro-lattices [16], composites with negative stiffness inclusions [17] and geometrically optimized periodic lattices [18,19].

Here, we report on novel architected materials with complex unit cell topologies, offering a combination of high stiffness, low transferred stress upon compression, and high energy dissipation coefficient resulting from rapid phase transformations of sub-unit-cell constituents under mechanical loads. The proposed architected materials exhibit an amount of energy dissipation per unit volume that approaches the theoretical maximum for any material and is nearly independent on the number of unit cells, offering much more compact designs than are possible with competing systems. This concept could significantly expand the performance of existing architected materials based on NS elements, and demonstrates a robust route to manufacturing reusable multifunctional dissipative systems that are comparable in performance to existing irreversible engineered materials.

When a chain of discrete elements with non-convex strain energy profile is compressed, instabilities can occur at prescribed overall displacements; the sudden structural changes assigned with these instabilities can be described as discrete phase transformations. During these transformations, some of the elements in the design will expand while others rapidly contract in order to release strain energy, leading the overall system to reconfigure into a lower-energy deformed state [20–22]. If the architected material is loaded under displacement control, this phenomenon is usually associated with an instantaneous drop in the applied load at a fixed displacement. The strain energy released in the form of kinetic energy of the phase transforming elements will be eventually dissipated to the environment through mechanical vibrations of the structural elements. Previously, it has been shown that (i) the specific value of the released strain energy (i.e., energy per element, unit cell, or volume) increases nonlinearly by increasing the number of discrete elements in the chain, N, reaching a plateau as $N \to \infty$; and (ii) a minimum number of rows of elements in a

* Corresponding author.
E-mail address: valdevit@uci.edu (L. Valdevit).

https://doi.org/10.1016/j.eml.2017.09.014
2352-4316/

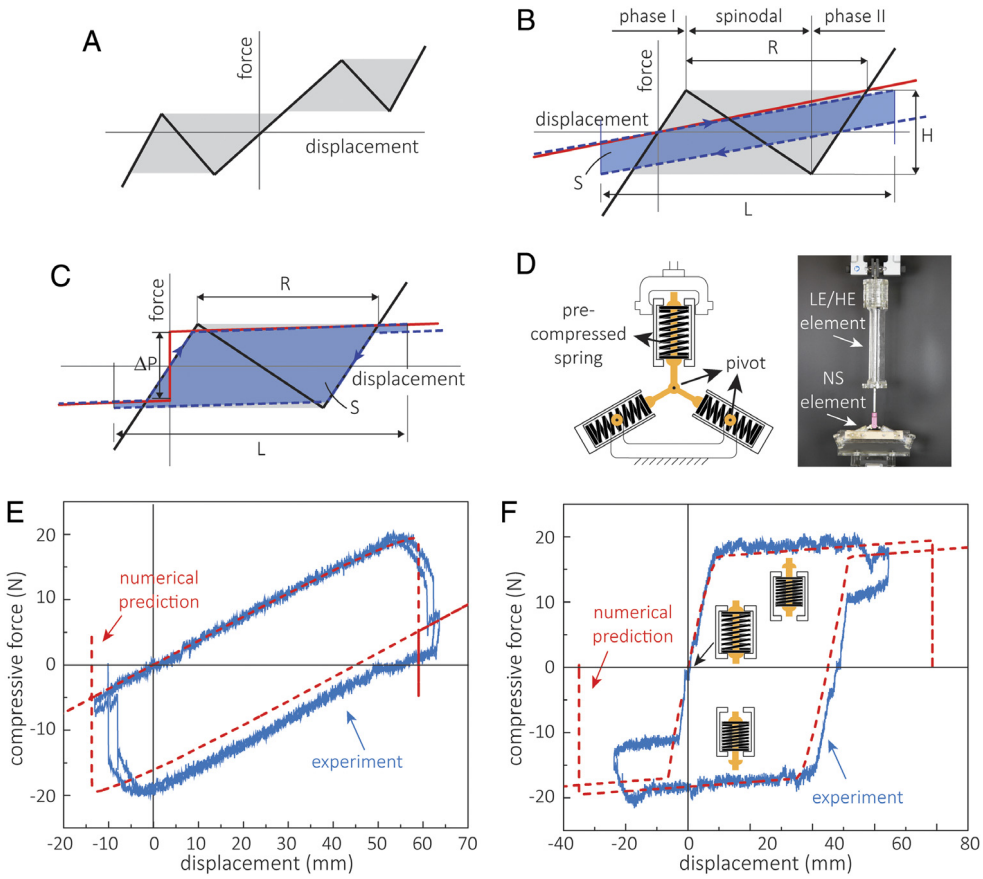

Fig. 1. (A) Schematic of a hypothetical force–displacement behavior for a non-convex elastic element encompassing two valleys; the shaded area denotes the absorption capacity of the discrete element within the displacement range shown. (B) Load–displacement curves of a linear elastic element (red), a NS element (black), and the associated collective response for a type I hybrid unit cell (dashed). (C) Load–displacement curves of a Heaviside elastic element (red), a NS element (black), and the associated collective response for a type II hybrid unit cell (dashed). (D) The experimental set-up for the simulation of the proposed type I and II architected materials. (E, F) Load–displacement behavior of type I and II hybrid unit cells, respectively, obtained experimentally (blue, two cycles) and numerically (red dashed). (For interpretation of the references to colour in this figure legend, the reader is referred to the web version of this article.)

chain is required to develop a non-zero hysteresis loop (and hence non-zero energy dissipation) [2]. Fig. 1A shows the schematic of a hypothetical force–displacement behavior for an elastic element with non-convex strain energy profile, with two valleys in the response. The shaded area in this figure corresponds to the maximum energy per element in a chain of N identical elements that can be elastically dissipated through hysteresis; this amount of energy can only be dissipated when $N \rightarrow \infty$. Henceforth, we refer to this area, which also denotes the maximum amount of energy (per cycle) that can be elastically absorbed from the kinetic energy of an oscillating object, as the theoretical absorption capacity of the non-convex element, and denote it by W_{th}. The ratio of the energy absorbed per unit element in an actual design, W_d, to the maximum absorbable energy is here defined as *absorption efficiency*, $\eta = W_d/W_{th}$.

2. Results and discussion

In Fig. 1B through F, we compare the dissipative performance of two different architected material designs with hybrid unit cells, differing by the mechanical characteristics of their sub-unit-cell components. The hybrid unit cell type I (Fig. 1B) is comprised of a linear elastic (LE) element (spring) arranged in series with a NS element (e.g., a pair of guided inclined beams). For the sake of simplicity and without loss of generality, it is assumed that the force–displacement profile in the two stable phases of response (phase I and II in Fig. 1B) for the NS element are parallel to each other, with R representing the horizontal distance between the two phases, and H denoting the height of the unstable (spinodal) phase. Fig. 1B shows the corresponding force–displacement curves of the LE element (red), and the NS element (black). The collective non-convex response of the stack obtained from our novel numerical algorithm (Movie SM1, Supplementary Information) is shown by dashed lines. The absorption capacity of the NS element is marked by the gray shaded area. Given a fixed force–displacement curve for the NS element (black), the resulting hysteresis area marked by the blue shaded region is only dependent on the stiffness of the linear element and is smaller than the absorption capacity of the NS element ($\eta \leq 1$). Our numerical analysis shows that the maximum efficiency $\eta = 1$ (i.e. $W_d = W_{th}$) is obtained when the stiffness of the linear element approaches zero. However, this requires cyclic loadings of infinitely large displacement amplitude, which renders realization of this maximum value practically impossible. Furthermore, decreasing the stiffness of the linear element greatly compromises the *specific damping capacity* of the material, $\Psi = W_d/W_s$, due to the more rapid growth of the stored elastic energy, W_s (sections 2 and 3, Supplementary Information).

In order to amend this critical shortcoming in the dissipative performance of nonconvex elastic systems, a large number of hybrid unit cells comprised of combinations, in series, of sub-unit-cell elements – herein simply referred to as elements – with varying stress–strain responses were constructed from a comprehensive library of discrete elements with convex and non-convex strain energy profiles, and their dissipative performance was numerically assessed (stress and strain are defined as load per unit cross sectional area and displacement per unit height of the unit cell,

respectively). Our numerical framework incrementally linearizes the total potential energy of the system of non-convex elements, and hence is much more efficient than previously proposed minimization schemes for optimization activities [5]. The proposed method is based on the assumption of quasi-static deformations, akin to an infinite damping condition, and finds the equilibrium and non-equilibrium paths corresponding to a stack (chain) of non-convex strain energy elements via an iterative procedure. At every increment, the overall length of the stack is varied, and the internal forces of the elements are updated accordingly. Equilibrium is checked by calculating the net forces acting at any degree of freedom in the system (the displacements of the midpoints of adjacent elements in the stack are independent degree of freedom). If the system is not in equilibrium (i.e., the net forces are not all identically 0), then the degrees of freedom are moved in the direction of (and by a magnitude proportional to) the net forces until equilibrium is reached. Stability per se is upheld by positive definiteness of the internal Hessian matrix of the system, D. In the case of non-positive-definiteness (i.e. instability), the internal degrees of freedom are incremented proportionally to the specific eigenvector of the matrix D which corresponds to the minimum eigenvalue, a direction that is proven to correspond to the maximum rate of decrease in the total potential strain energy of the system. A more comprehensive discussion about the algorithm is reported in Section 1 of the Supplementary Information.

Specifically, it was discovered that a convex elastic element with a trilinear force–displacement behavior encompassing a phase of high stiffness surrounded by two phases of compliant behavior under both tension and compression (henceforth referred to as a Heaviside elastic element (HE) – red curve in Fig. 1C), arranged in series with a NS element (black curve in Fig. 1C), results in a hybrid unit cell with superior levels of energy dissipation efficiency. We call this arrangement hybrid unit cell type II. Fig. 1C shows the corresponding force–displacement curves of the trilinear HE element in red, a typical NS element in black, and the collective non-convex response obtained from our numerical analysis in dashed (Movie SM2, Supplementary Information). Similar to the case of the hybrid unit cell type I, the NS element (black) allows multiple stable phases with different strain energy for the hybrid unit cell, and its snap-through results in transitions between lower- and higher-energy modes. The force–displacement behavior of HE element (red) starts with a relatively stiff slope, then assumes a rather compliant behavior (or plateau), analogous to the behavior of an elastic-perfectly plastic material. Note that in an elastic-perfectly plastic material the loading and unloading paths are not coincident, due to material intrinsic energy dissipation. Here, however, the HE element, and hence the type II hybrid unit cell, are fully elastic and the HE element traverses the same path during loading and unloading. Notably, the plateau strength of the HE element is chosen to be slightly lower than the snap-through strength of the NS element, a condition needed to ensure significant deformation in the HE element before the NS element snaps through. The HE element serves two major functions: (i) it curbs the level of stress within the architected material and therefore the stress transferred to the protected system, and (ii) it maintains sufficient load (compressive under overall compression and tensile under overall tension) in the structure to enable phase transformation of the NS element(s) at almost constant stress. As shown by the blue area in Fig. 1C, a significant amount of energy dissipation (area inside the hysteresis loop) is enabled by the proposed type II hybrid unit cell.

We have corroborated these findings experimentally in Fig. 1D through F. In a prototype type II unit cell, shown in Fig. 1D, a near-sinusoidal snap-through behavior for the NS element is obtained by a pair of inclined springs pin jointed to a rigid base at the bottom of the cell. The HE element (displayed above the NS element) is realized by a pre-compressed elastic spring which is fitted inside a rigid metallic cylindrical frame (section 4, Supplementary Information). The combination of these sub-unit-cell elements in series is the hybrid type II cell described above. At the same time, by setting the value of the pre-stress in the top spring equal to zero, the HE element reverts to a simple linear spring, and hybrid unit cell type I is obtained.

The associated force–displacement hysteresis behavior of the hybrid units type I and II under cyclic loading is shown in Fig. 1E and 1F, respectively. Notice that the type II hybrid unit cell prototype enables remarkable energy absorption efficiency of $\eta = 0.91$ and specific damping capacity of $\psi = 6.02$, considerably above the reported range of dissipation in high damping elastomers ($\psi < 4.5$) [23]. For comparison, the type I hybrid unit cell prototype shows energy absorption efficiency of $\eta = 0.65$ and specific damping capacity of $\psi = 3.52$. Moreover, the type II unit cell is about 10 time stiffer than the type I unit cell. The insets in Fig. 1F show configurations of the spring within the HE element during different phases of the response. The results are in good agreement with the results from numerical simulation shown by red dashed line in these set of figures.

There are interesting distinctions between the performance characteristics of the two proposed architected hybrid material systems. First, the type II hybrid design can provide a much higher initial stiffness; the application of linear springs within the architected materials (as in the type I hybrid design) renders the structure excessively compliant and thus unsuitable in many applications. This difference between the initial stiffness values in these two hybrid designs becomes especially substantial if the NS behavior is implemented via a buckling-driven setup with stretching dominated initial response (e.g., a pair of inclined beams). Furthermore, for prescribed values of dissipated energy and cyclic displacement (stroke) amplitude (denoted as S and L in Fig. 1B and C), the maximum stress in the type II hybrid design is significantly smaller than that of hybrid design type I (Figure S4, Supplementary Information). This distinction makes the type II design strongly desirable for impact protection applications, where maximum energy dissipation at a relatively low stress transfer level is a defining metric. Finally, even though both type I and II hybrid designs are theoretically able to provide comparable values of ψ, the type I design requires a much larger stroke, especially as the desired absorption efficiency approaches unity, $\eta \to 1$. It can be shown that the following relationships hold for the absorption efficiency of type I and type II elastic architected materials (see section 2, Supplementary Information):

$$\eta^{I} = \frac{\left(\frac{L}{R}\right)}{1+\left(\frac{L}{R}\right)} \qquad 0 < L/R < \infty \tag{1}$$

$$\eta^{II} = \frac{\left(\frac{L}{R}\right) + \frac{\Delta P}{H} \times \min\left(1,\ \left(\frac{L}{R}\right)^2\right)}{1+\left(\frac{L}{R}\right)} \qquad 0 < L/R < \infty \tag{2}$$

Eq. (2) will be simplified to Eq. (1) when $\Delta P/H = 0$.

Fig. 2A and B compare important dissipation characteristics of the two proposed hybrid unit cells. Fig. 2A shows the contour plot of the displacement amplitude (stroke) ratio, defined as the ratio of the displacement amplitude of hybrid unit cell II, L_2, to that of hybrid unit cell I, L_1, versus the normalized values of width of the step function in hybrid unit cell II, $\Delta P/H$ (see Fig. 1C), and absorption efficiency, η. Note that if ΔP approaches zero, element type II converges to element type I, and the stroke ratio approaches unity. As evident from the upper right corner of the map, significantly shorter strokes are needed in a type II hybrid unit cell compared to a type I hybrid unit cell to obtain the optimal hysteresis area of $\eta \approx 1$.

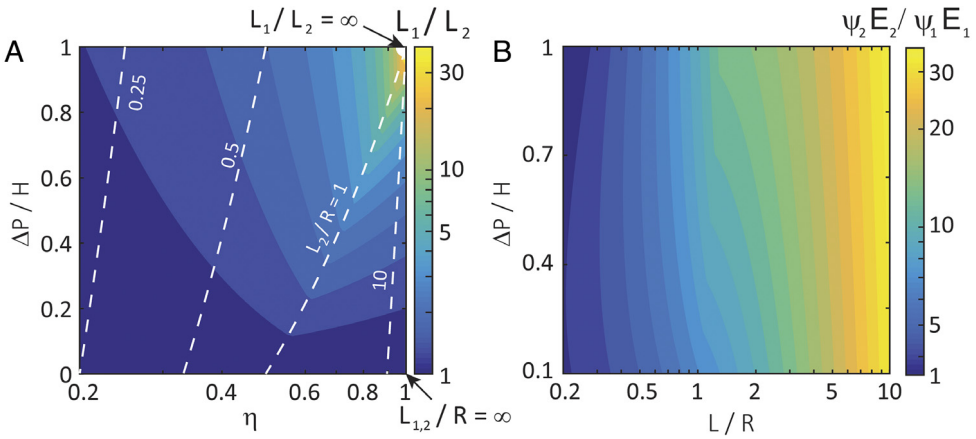

Fig. 2. Design maps for important dissipation characteristics of the proposed type I and II hybrid unit cells. (A) Contour plot of the displacement amplitude ratio, L_1/L_2, for different normalized values of height of the Heaviside step function in the hybrid element type II, $\Delta P/H$, and absorption efficiency, η. (B) Contour plot of the ratio of the material selection index $M_d = \Psi E$, for different normalized values of the width of the Heaviside step function in hybrid element II, $\Delta P/H$, and displacement amplitude, L/R. In this set of results, $\overline{K}^I = K^I/K^* = 5$ (cf. inset of Fig. 3).

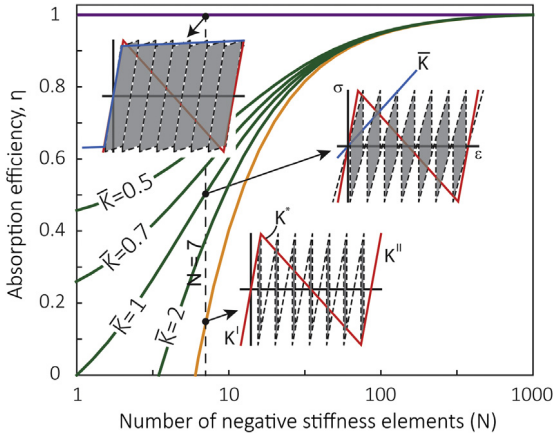

Fig. 3. Absorption efficiency, η, versus number of negative stiffness elements, N, in a chain of discrete elements with non-convex strain energy. The negative stiffness elements (red curve in the insets) are assumed to have a trilinear stress–strain response (slopes K^I, K^*, K^{II} from left to right), with equal slopes in phases I and II ($K^I = K^{II}$). In this set of results, $\overline{K}^I = K^I/K^* = 5$. Results are shown for the following cases: (i) a pure chain of negative stiffness elements (orange), (ii) the stack in (i) in series with one linear elastic element of normalized slope $\overline{K} = 0.5$, 0.7, 1 and 2, where $\overline{K} = K/K^*$ (green), (iii) the stack in (i) in series with one Heaviside elastic element (purple). (For interpretation of the references to colour in this figure legend, the reader is referred to the web version of this article.)

It is also useful to examine the advantages of the proposed structures in vibration management applications. A relevant figure of merit for vibration suppression in foams and cores of sandwich panels under broad-band inputs is $M_d = \Psi E$, where Ψ is the damping coefficient, and E is the Young's modulus (stiffness) of the architected material [24]. Fig. 2B shows contours of the ratio of the index M_d for type I and type II unit cells, i.e., $\Psi_2 E_2/\Psi_1 E_1$, versus the normalized values of width of the step function in the hybrid unit cell II, $\Delta P/H$, and displacement amplitude, L/R. Notice that the materials index in a type II hybrid unit cell can be up to ∼30 times higher, demonstrating the superiority of the type II unit cell in vibration suppression.

It is instructive to compare the energy dissipation capacity of the proposed architected materials as the number of NS elements in the stack of elements increases. Fig. 3 shows the energy absorption efficiency, η, versus the number of NS elements within the stack for various types of architected material designs. First, consider an architected material where the stack consists of N identical NS elements, whose energy dissipation capacity has been previously studied (orange curve) [2]. As previously demonstrated, there is a minimum number of NS elements needed in order for hysteretic behavior to ensue; for architected materials with fewer unit cells than this critical number, no energy is dissipated upon cyclic loading, and the unloading path, albeit non-linear, perfectly coincides with the loading path. This critical number is dependent on the stress–strain characteristics of the NS elements, and for the case of NS elements with trilinear stress–strain behavior is equal to $1 + \overline{K}^I$, where $\overline{K}^I$ is the normalized stiffness in the phase I (and II) of response (section 2c, Supplementary Information). The other curves in Fig. 3 represent the dissipative response of architected materials with hybrid unit cells discussed in this work. The green curves present the performance of type I (linear) hybrid designs, for different values of the normalized stiffness of the linear elastic element, $\overline{K}$. Notice that while a lower value of $\overline{K}$ results in improved damping efficiency, reducing $\overline{K}$ might make the structure excessively compliant. Finally, the purple curve shows the absorption efficiency of a type II architected material, which is almost independent of the number of NS elements in the stack. The benefits of the type II design in terms of energy absorption efficiency are evident from this figure: a type II hybrid material design with a single unit cell has the same absorption efficiency as 1000 negative stiffness elements in series. This result can have profound implications on the design of reversible impact resistant structures. It is also interesting to note that the addition of a single HE element can significantly increase the absorption efficiency of a chain of otherwise identical NS elements. This is simply due to the fact that only one NS element at a time would experience phase transformation during both loading and unloading, which allows the HE element to *reset* after each NS element phase transformation. A reset HE element is squeezed (or expanded) enough to maintain an almost constant chain load during the phase transformation of the NS element (Movie SM3, Supplementary Information). The consecutive transformation of NS elements is not only due to the structural imperfections that would practically render the NS elements non-identical, but also to allow the maximum rate of decrease of the total potential energy in ideal systems [20,22].

It is useful to examine design and fabrication strategies to implement the proposed concept in the form of a scalable periodic architected material, rather than a device or a mechanism, particularly in light of the complexities involved in incorporating the spring setup shown in Fig. 1D into a 3D architected material. Several methods have been previously proposed to obtain NS effects through structural nonlinearity, including use of inclined guided

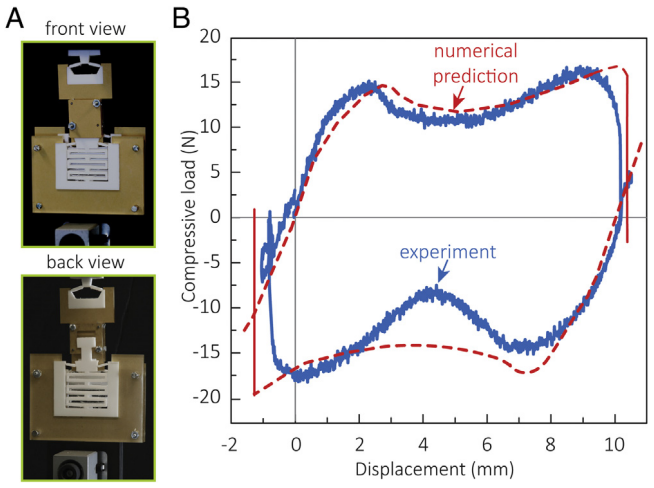

Fig. 4. A scalable type II hybrid unit-cell design for construction of a large-scale architected material (left), and the corresponding load–displacement response (right). Numerical simulations obtained with our code (red) are in good agreement with experimental results (blue). (For interpretation of the references to colour in this figure legend, the reader is referred to the web version of this article.)

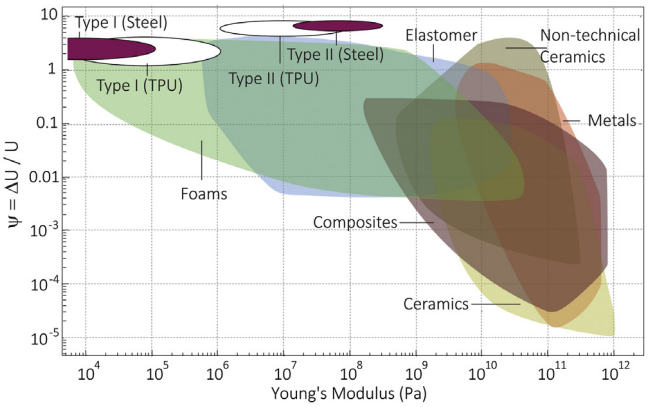

Fig. 5. Materials selection chart of specific damping capacity, ψ, versus Young's modulus, E, for the universe of existing materials and the proposed type I and II architected elastic materials. Results are provided for two representative constituent materials, a metal (steel), and a polymer (TPU).

beams [4,25], arches [26], pre-stressed buckled beam [27], and columns with edge contact [28]. Here, we choose inclined guided beams due to their initial stretching dominated response and significant elastic displacements. The HE element is implemented via the superposition in parallel of a typical negative stiffness element with an element with positive linear response (section 4a, Supplementary Information). The complete implementation of the type II hybrid unit cell is shown in Fig. 4A. It consists of deformable, laser cut pieces of PTFE (Teflon) with $E = 500$ MPa, $\nu = 0.45$, and high yield strain of 3–5% (white), and relatively stiff laser cut pieces of acrylic (brown), whose function is to connect or laterally constrain the deforming Teflon parts. The hybrid unit cell consists of a parallel arrangement of two (front and back) sets of Teflon parts each constrained by U-shaped acrylic pieces, simulating a bottom HE element, which are placed in series with a NS element on top (section 4b, Supplementary Information). To demonstrate the feasibility of the proposed architecture, in Fig. 4B we have shown the experimental force–displacement response of the hybrid unit cell under quasi-static loading. The results from the simulation are also shown by a red dashed curve. In order to obtain the numerical results, first the bottom HE and the top NS elements are separately tested under quasi-static loading ($\dot{\varepsilon} = 10^{-4}$ s^{-1}) to obtain their load–displacement response. Next, the experimental curve data points are plugged into the numerical code (section 1, Supplementary Information) to obtain the overall response curve. The discrepancies between the numerical and experimental results could be attributed to misalignments and out-of-plane movements of the assembled hybrid structure in series ($N = 2$) compared to each individual component, and also to perturbations during testing that cause the non-convex system to avoid peaks of potential energy and become unstable (characterized by sharp drops in load) at lower displacement than predicted by the numerical model. This particular type II hybrid design implementation exhibits a specific damping capacity of $\psi = 5.43$ and an absorption efficiency of $\eta = 0.79$.

Although the merits of the proposed design have been clearly presented, an outstanding question is whether the dissipative performance of the proposed hybrid material system is comparable to that of existing materials that absorb energy based on destructive modifications (whether in foams, bulk materials or structures). Fig. 5 shows a material selection "Ashby" map of specific damping capacity, Ψ, versus Young's modulus, E, for the universe of existing materials. For general dissipation and vibration management purposes, materials in the top right corner of the map would be optimal [29]. Also presented is the performance of the type I and II hybrid unit cell designs, encompassing two NS element ($N = 2$) and made of thermoplastic polyurethane (TPU) and steel constituent material. Notice that the proposed type II hybrid material outperforms all existing engineered and natural materials in terms of energy dissipation, while maintaining a Young's modulus comparable to that of polymers and elastomers.

3. Discussion

In summary, we propose a new class of architected materials with hybrid unit cells consisting of discrete elastic elements with non-convex strain energy and one convex (but possibly nonlinear) elastic element, to obtain a reversible effective multifunctional material with remarkable energy dissipation, relatively high stiffness, and low transmitted stress, in a compact design. The proposed design exploits numerically optimized nonlinearities in the force–displacement response of the sub-unit-cell elements to approach the theoretical limit of specific damping capacity in materials, $\psi^{th} = 8$, under quasi-static loading. Specific damping capacities up to $\psi = 6.02$ were experimentally demonstrated, which are far greater than any experimental value previously reported [30–32]. Furthermore, a distinct advantage of the proposed elastic architected materials is their reversibility and reusability after deformation, resulting in increased life-span.

All hybrid unit-cell prototypes presented in this article are bistable, and therefore recoverability under unidirectional loading (e.g. impact) is not automatic; subsequent external actuation in the reverse direction is needed for recovery. However, the proposed architected materials can be designed single-stable, and hence automatically recoverable, with hysteresis still present in the force–displacement curve. To this end, one can use a linear spring *in parallel* with the proposed type I or type II hybrid unit cells, such that the overall force–displacement response of the resulting unit cell becomes single stable. This approach would not affect the amount of hysteresis (area inside the curve) or absorption efficiency, η, for a given displacement cycle, but will compromise the specific damping capacity, ψ, of the material unit cell [15]. An alternative method towards single-stability and recoverability is by manipulating the geometry of the employed NS elements [1,4]. Even though a single unit cell in both of these cases will not exhibit any hysteresis or energy dissipation during a full displacement

cycle or a unidirectional loading event, a stack of single-stable unit cells will still exhibit hysteresis according to the mechanism described in this article (subject to the condition on the minimum number of cells—see Fig. 3).

The materials proposed herein can potentially lead to enhancements in crashworthiness and energy absorption under dynamic loading events, such as impact, compared to previously proposed energy absorbent elastic materials that reduce the kinematic energy of the projectile through trapping of strain energy [1] or multi-cell dynamic effects [2]. Nevertheless, the current study has only examined the behavior of the proposed structure under quasi-static loading, and further studies are needed to assess strain rate and frequency dependencies. When the imposed macroscopic crushing strain rate, $\dot{\varepsilon}$, is much smaller than the minimum natural frequency the hybrid unit cell (pertaining to its internal degree of freedom), ω_n, such effect are expected to be negligible (see [15] for a detailed analysis).

Acknowledgments

Funding from Office of Naval Research (Program Manager: D. Shifler, Contract # N000141110884) is gratefully acknowledged. The Abaqus® Finite Element Analysis software is licensed from Dassault Systemes SIMULIA, as part of a Strategic Academic Customer Program between UC Irvine and SIMULIA.

Appendix A. Supplementary data

Supplementary material related to this article can be found online at https://doi.org/10.1016/j.eml.2017.09.014.

References

[1] S. Shan, S.H. Kang, J.R. Raney, P. Wang, L. Fang, F. Candido, J.A. Lewis, K. Bertoldi, Multistable architected materials for trapping elastic strain energy, Adv. Mater. 27 (2015) 4296–4301. http://dx.doi.org/10.1002/adma.201501708.
[2] D. Restrepo, N.D. Mankame, P.D. Zavattieri, Phase transforming cellular materials, Extrem. Mech. Lett. 4 (2015) 52–60. http://dx.doi.org/10.1016/j.eml.2015.08.001.
[3] T. Frenzel, C. Findeisen, M. Kadic, P. Gumbsch, M. Wegener, Tailored buckling microlattices as reusable light-weight shock absorbers, Adv. Mater. 28 (2016) 5865–5870. http://dx.doi.org/10.1002/adma.201600610.
[4] B. Haghpanah, L. Salari-Sharif, P. Pourrajab, J. Hopkins, L. Valdevit, Multistable shape-reconfigurable architected materials, Adv. Mater. 28 (2016) 7915–7920. http://dx.doi.org/10.1002/adma.201601650.
[5] K. Che, C. Yuan, J. Wu, H.J. Qi, J. Meaud, Three-dimensional-printed multistable mechanical metamaterials with a deterministic deformation sequence, J. Appl. Mech. 84 (2017) 011004. http://dx.doi.org/10.1115/1.4034706.
[6] T. Hewage, K.L. Alderson, A. Alderson, F. Scarpa, Double-negative mechanical metamaterials displaying simultaneous negative stiffness and negative Poisson's ratio properties, Adv. Mater. 28 (2016) 10323–10332. http://dx.doi.org/10.1002/adma.201603959.
[7] A. Rafsanjani, D. Pasini, Bistable auxetic mechanical metamaterials inspired by ancient geometric motifs, Extrem. Mech. Lett. 9 (2016) 291–296. http://dx.doi.org/10.1016/j.eml.2016.09.001.
[8] L. Dong, R.S. Lakes, Advanced damper with negative structural stiffness elements, Smart Mater. Struct. 21 (2012) 75026. http://dx.doi.org/10.1088/0964-1726/21/7/075026.
[9] C.B. Churchill, D.W. Shahan, S.P. Smith, A.C. Keefe, G.P. Mcknight, Dynamically variable negative stiffness structures, Sci. Adv. 2 (2016) 1–7. http://dx.doi.org/10.1126/sciadv.1500778.
[10] X. Liu, X. Huang, H. Hua, On the characteristics of a quasi-zero stiffness isolator using Euler buckled beam as negative stiffness corrector, J. Sound Vib. 332 (2013) 3359–3376. http://dx.doi.org/10.1016/j.jsv.2012.10.037.
[11] B.A. Fulcher, D.W. Shahan, M.R. Haberman, C.C. Seepersad, P.S. Wilson, Analytical and experimental investigation of buckled beams as negative stiffness elements for passive vibration and shock isolation systems, J. Vib. Acoust. 136 (2015) 12. http://dx.doi.org/10.1115/1.4026888.
[12] D.L. Platus, Negative-stiffness-mechanism vibration isolation systems, Control 1619 (1991) 0–8. http://dx.doi.org/10.1117/12.56823.
[13] N. Nadkarni, A.F. Arrieta, C. Chong, D.M. Kochmann, C. Daraio, Unidirectional transition waves in bistable lattices, Phys. Rev. Lett. 116 (2016) 1–5. http://dx.doi.org/10.1103/PhysRevLett.116.244501.
[14] J.R. Raney, N. Nadkarni, C. Daraio, D.M. Kochmann, J.A. Lewis, K. Bertoldi, Stable propagation of mechanical signals in soft media using stored elastic energy, Proc. Natl. Acad. Sci. 113 (2016) 9722–9727. http://dx.doi.org/10.1073/pnas.1604838113.
[15] A. Guell Izard, R. Fabian Alfonso, G. McKnight, L. Valdevit, Optimal design of a cellular material encompassing negative stiffness elements for unique combinations of stiffness and elastic hysteresis, Mater. Des. 135 (2017) 37–50. http://dx.doi.org/10.1016/j.matdes.2017.09.001.
[16] L. Salari-Sharif, T.A. Schaedler, L. Valdevit, Energy dissipation mechanisms in hollow metallic microlattices, J. Mater. Res. 29 (2014) 1755–1770. http://dx.doi.org/10.1557/jmr.2014.226.
[17] F. Fritzen, D.M. Kochmann, Material instability-induced extreme damping in composites: A computational study, Int. J. Solids Struct. 51 (2014) 4101–4112. http://dx.doi.org/10.1016/j.ijsolstr.2014.07.028.
[18] S. Krödel, L. Li, A. Constantinescu, C. Daraio, Stress relaxation in polymeric microlattice materials, Mater. Des. 130 (2017) 433–441. http://dx.doi.org/10.1016/j.matdes.2017.05.060.
[19] A. Asadpoure, M. Tootkaboni, L. Valdevit, Topology optimization of multiphase architected materials for energy dissipation, Comput. Methods Appl. Mech. Engrg. 325 (2017) 314–329. http://dx.doi.org/10.1016/j.cma.2017.07.007.
[20] I. Benichou, S. Givli, Structures undergoing discrete phase transformation, J. Mech. Phys. Solids 61 (2013) 94–113. http://dx.doi.org/10.1016/j.jmps.2012.08.009.
[21] F. Fraternali, T. Blesgen, A. Amendola, C. Daraio, Multiscale mass–spring models of carbon nanotube foams, J. Mech. Phys. Solids 59 (2011) 89–102. http://dx.doi.org/10.1016/j.jmps.2010.09.004.
[22] G. Puglisi, L. Truskinovsky, Mechanics of a discrete chain with bi-stable elements, J. Mech. Phys. Solids 48 (2000) 1–27. http://dx.doi.org/10.1016/S0022-5096(99)00006-X.
[23] Granta Design, Cambridge Engineering Selector (CES) software, 1999.
[24] M.F. Ashby, Materials selection in mechanical design, 2013. http://dx.doi.org/10.1017/cbo9781107415324.004.
[25] J. Zhao, J. Jia, X. He, H. Wang, Post-buckling and snap-through behavior of inclined slender beams, J. Appl. Mech. 75 (2008) 41020. http://dx.doi.org/10.1115/1.2870953.
[26] J. Qiu, J.H. Lang, A.H. Slocum, A curved-beam bistable mechanism, J. Microelectromech. Syst. 13 (2004) 137–146. http://dx.doi.org/10.1109/JMEMS.2004.825308.
[27] M. Vangbo, An analytical analysis of a compressed bistable buckled beam, Sensors Actuators A 69 (1998) 212–216. http://dx.doi.org/10.1016/S0924-4247(98)00097-1.
[28] L. Dong, R. Lakes, Advanced damper with high stiffness and high hysteresis damping based on negative structural stiffness, Int. J. Solids Struct. 50 (2013) 2416–2423. http://dx.doi.org/10.1016/j.ijsolstr.2013.03.018.
[29] H.N. Ashby, Michael F. Evans, Anthony Fleck, Norman A. Gibson, Lorna J. Hutchinson, John W. Wadley, Metal foams: a design guide, 2000. http://dx.doi.org/10.1016/S0261-3069(01)00049-8.
[30] L.R. Meza, S. Das, J.R. Greer, Strong, lightweight, and recoverable three-dimensional ceramic nanolattices, Science 345 (2014) 1322–1326. www.sciencemag.org/content/345/6202/1322/suppl/DC1.
[31] L.R. Meza, A.J. Zelhofer, N. Clarke, A.J. Mateos, D.M. Kochmann, J.R. Greer, Resilient 3D hierarchical architected metamaterials, Proc. Natl. Acad. Sci. USA 112 (2015) 11502–11507. http://dx.doi.org/10.1073/pnas.1509120112.
[32] T.A. Schaedler, A.J. Jacobsen, A. Torrents, A.E. Sorensen, J. Lian, J.R. Greer, L. Valdevit, W.B. Carter, Ultralight metallic microlattices, Science 334 (80) (2011) 962–965. http://dx.doi.org/10.1126/science.1211649.